
Efficient Formulations of Heat and Mass Transfer in Oil Shale Retort Models

Jack C. Parker and Fan Zhang

*Oak Ridge National Laboratory, PO Box 2008, Oak Ridge TN 37831-6036
parkerjc@ornl.gov*

Abstract

A mathematical model for oil shale retorting is described that considers kerogen pyrolysis, oil coking, residual carbon gasification, carbonate mineral decomposition, water-gas shift, and phase equilibria reaction. Reaction rate temperature-dependence is described by Arrhenius kinetics. Fractured rock is modeled as a bi-continuum consisting of fracture porosity in which advective and dispersive gas and heat transport occur, and rock matrix in which diffusive mass transport and thermal conduction occur. Heat transfer between fracture and matrix regions is modeled either by a partial differential equation (PDE) for spherical conduction or by a linear first-order heat transfer formulation. Mass transfer is modeled in an analogous manner or assuming local equilibrium. First-order mass and heat transfer coefficients are computed by a theoretical model from fundamental rock matrix properties. The governing equations are solved using a 3-D finite element formulation. Simulations of laboratory retort experiments and hypothetical problems indicated thermal disequilibrium to be the dominant factor controlling retort reactions. Simulation accuracy was unaffected by choice of mass transfer formulation. However, computational effort to explicitly simulate diffusive mass transfer in the rock matrix increased computational effort by more than an order of magnitude compared with first-order mass transfer or equilibrium analyses. A first-order heat transfer approximation of thermal conduction can be used without significant loss of accuracy if the block size and/or heating rate are not too large, as quantified by a proposed dimensionless heating rate.

Background

Due to the very low native permeability of oil shales, most production schemes involve induced fracturing by fluid over-pressuring, thermal shocking, and/or explosives to create permeable fracture porosity within a matrix of low permeability rock fragments. Fluid flow is largely confined to fractures with diffusion-controlled mass transfer between fractures and rock fragments. Advective heat transfer predominates within the fracture porosity, while thermal conduction controls heat transfer between fractures and rock fragments, which in turn governs rates of pyrolysis and other reactions within the rock matrix. Differences in rock fragment size (or fracture spacing) affect the degree of thermal and chemical disequilibrium between fracture and rock matrix regions, which in turn strongly impact oil production efficiency (Tyner and

Cook, 1984; Tyner et al., 1985; and Suduth et al., 1987).

Computer models applicable to *in situ* oil shale retorting have been reported and applied to analyze bench scale and field pilot tests under various conditions (George and Harris, 1977; Gregg et al., 1981; Libicki and Campbell, 1980; Campbell et al., 1980; Braun, 1981; Braun et al., 1982). Previous oil shale modeling efforts have utilized a multi-continuum modeling approach involving a primary continuum representing fracture porosity and one or more secondary continua representing rock fragments. For each secondary continua representing a given rock fragment size, partial differential equations for heat and mass transfer may be formulated and solved numerically, requiring spatial discretization of each rock size class at each computational location in

the primary continuum. Thus, if the primary continuum is discretized into N computational nodes, and each of M rock size classes is discretized into P nodes (e.g., radial coordinates for assumed spherical fragments), a total of NxMxP computational nodes must be solved for the governing heat and reactive mass transport equations. For field-scale 3-D problems involving tens or hundreds of thousands of nodes in the primary fracture continuum, the total number of nodes can conservatively increase by a factor of 100 or more. Furthermore, because time-constants for heat and mass transfer processes in fractures and rock fragments differ substantially, finer temporal discretization may be required, further increasing computational effort and increasing the likelihood of convergence and accuracy problems.

This paper focuses on the development and testing of more efficient formulations to simulate heat and mass transfer processes in rubbleized oil shale during *in situ* retorting.

Model Description

Overview

The retort zone is modeled as a dual-continuum medium consisting of rock fragments and a continuous fracture network.

Rock fragments are idealized as impermeable spherical bodies. Gas phase flow is considered within the fracture continuum only. In this study, liquid phase flow is not considered. Processes considered within each continuum are summarized in Table 1. A summary of the reaction network is given in Table 2. The numerical model was implemented using a modified version of the 3-D finite element code HGC5 (Yeh et al, 2004).

Fracture-Rock Matrix Mass Transfer

Three approaches are investigated for modeling mass transfer between fractures and rock matrix continua:

Method 1: Spherical Diffusion Model. In this approach, each computational node in the fracture continuum is coupled to a partial differential equation (PDE) for diffusion in adjacent rock fragments. Assuming approximately equi-dimensional rock fragments, spherical symmetry is assumed to reduce dimensionality of the numerical problem to

$$\frac{\partial(C_{mi}\phi_m)}{\partial t} = \frac{1}{r^2} \frac{\partial}{\partial r} \left(D_{mi} r^2 \frac{\partial C_{mi}}{\partial r} \right) + R_{mi} \quad (1)$$

where C_{mi} is the gas phase concentration of species i in the rock matrix, ϕ_m is the gas phase volume within the rock matrix per total fracture-matrix volume, D_{mi} is an ef-

Table 1: Processes modeled in fracture and matrix continua

Process	Fractures	Rock Matrix
Fluid flow	x	
Advective mass transport	x	
Dispersive mass transport	x	
Diffusive mass transport	x	x
Advective heat transport	x	
Thermal conduction	x	x
Pyrolysis		x
Carbon gasification		x
Mineral decomposition		x
Oil coking		x
Water-gas shift	x	x
Bound water loss		x
Water distillation/condensation	x	x
Oil distillation/condensation	x	x

Table 2: In situ retort reaction network

Description	Reaction ¹	Kinetics
Primary pyrolysis	$\text{kerogen}_{(s)} \rightarrow \text{oil}_{(l)} + \text{gas}_{(v)} + \text{H}_{2(v)} + \text{CH}_{4(v)} + \text{CO}_{2(v)} + \text{H}_2\text{O}_{(v)} + \text{char1}_{(s)}$	Arrhenius (Campbell et al., 1980)
Secondary pyrolysis	$\text{char1}_{(s)} \rightarrow \text{H}_{2(v)} + \text{CH}_{4(v)} + \text{char2}_{(s)}$ $\text{char2}_{(s)} \rightarrow \text{H}_{2(v)} + \text{ROC}_{(s)} + \text{ROH}_{(s)}$	Arrhenius with normally distributed activation energies ² (Campbell, 1980)
Carbon gasification	$\text{ROC}_{(s)} + \text{CO}_{2(v)} \rightarrow \text{CO}_{(v)}$	Ergun (Gregg et al., 1981; Braun, 1981)
Dolomite decomposition	$\text{MgCa}(\text{CO}_3)_{2(s)} \rightarrow \text{CaCO}_{3(s)} + \text{MgO}_{(s)} + \text{CO}_2_{(v)}$	Arrhenius (Gregg et al., 1981)
Calcite decomposition	$\text{CaCO}_{3(s)} + \text{SiO}_{2(s)} \rightarrow \text{Ca}_2\text{SiO}_{4(s)} + \text{CaO}_{(s)} + \text{CO}_{2(v)}$	Arrhenius (Braun, 1981)
Oil coking	$\text{oil}_{(l)} \rightarrow \text{H}_{2(v)} + \text{CH}_{4(v)} + \text{ROC}_{(s)} + \text{coke}_{(s)}$	Arrhenius (Braun, 1981)
Water-gas shift	$\text{CO}_{(v)} + \text{H}_2\text{O}_{(v)} \rightarrow \text{CO}_{2(v)} + \text{H}_{2(v)}$	First-order in all species (Braun, 1981)
Bound water floss	$\text{H}_2\text{O}_{(s)} \rightarrow \text{H}_2\text{O}_{(v)}$	Constant rate from 120-360 °C (Braun, 1981)
Water distillation/condensation	$\text{H}_2\text{O}_{(l)} \rightarrow \text{H}_2\text{O}_{(v)}$	Equilibrium
Oil distillation/condensation	$\text{oil}_{(l)} \rightarrow \text{oil}_{(v)}$	Equilibrium

¹ stoichiometry not shown
² char1 and char2 each represented by 7 pseudo-species with activation energies equal to the mean and ± 0.5 , ± 1.5 , ± 2.5 standard deviations from the mean.

fective gas phase molecular diffusion coefficient of species i in the rock matrix, R_{mi} is the rate of species i production (+) or loss (-) due to reactions within the rock matrix per total fracture-matrix volume, and r is radial distance from the center of a rock fragment (C_{mi} , D_{mi} and R_{mi} vary with radial location and time). Equation (1) is subject to the boundary condition that C_{mi} at the outer radius of the rock fragment is equal to the concentration in the fracture continuum at the corresponding fracture node. The initial rock matrix porosity is assumed to be 0.01 and the magnitude is updated with time due to reactions that result in solid phase losses (e.g., pyrolysis). The effective diffusion coefficient is computed from the Millington-Quirk model as

$$D_{mi} = D_{oi} \phi_m^{10/3} \phi_{mi}^{-2} \quad (2)$$

where D_{oi} is the molecular diffusion coefficient of species i in bulk gas at the local rock temperature, and ϕ_{mi} is the ultimate pore volume in the rock following removal of kerogen per total fracture-matrix volume.

The net mass transfer rate for species i from the matrix continuum to fractures (+) or visa versa (-), M_{fmi} , which is a source-sink term in the fracture mass balance equations, is given by

$$M_{fmi} = R_{mi} - \frac{dC_{mi} \phi_m}{dt} \quad (3)$$

where the overbar signifies an average over the matrix region such that

$$\overline{C_{mi}\phi_m} = \frac{3}{r_m^3} \int_0^{r_m} r^2 C_{mi}\phi_m dr. \quad (4)$$

where r_m is the radius of rock fragments. To consider a distribution of rock fragment sizes, additional rock matrix continua must be added to the system of equations for each size class considered. Each rock matrix PDE must be discretized in the radial dimension at each fracture node for numerical solution of the coupled reactive heat/mass transport model.

Method 2: First-Order Mass Transfer Model.

This approach replaces the rock matrix PDEs with linear mass transfer functions as

$$M_{fmi} = \alpha_i (\overline{C_{mi}} - C_{fi}) \quad (5)$$

where α_i is a mass transfer coefficient for species i , C_{fi} is the gas phase concentration of species i in the fracture continuum,

$$\overline{C_{mi}} = \overline{C_{mi}\phi_m} / \overline{\phi_m}$$

is average matrix concentration of species i , and $\overline{\phi_m}$ is the average gas phase volume in the matrix per total matrix-fracture volume. Parker and Valocchi (1986) have shown that the spherical diffusion and first-order mass transfer models produce identical second moments when the mass transfer coefficient is defined by

$$\alpha_i = \frac{15\overline{D_{mi}}}{r_m^2} \quad (6)$$

where $\overline{D_{mi}}$ is the average effective diffusion coefficient in the rock matrix, which we compute from equation (2) using the average rock matrix temperature. Equations (5) and (6) represent a linearized approximation of diffusive transport, in which the mass transfer coefficient is defined wholly in terms of diffusion model parameters.

Method 3: Instantaneous Mass Transfer. If reaction rates in the rock matrix are primarily limited by fracture-matrix heat transfer rates rather than by mass transfer limitations, then it may be feasible to disregard fracture-matrix mass transfer proc-

esses. In this case, reaction rates in the rock matrix are applied directly as source-sink terms in the fracture mass balance equation and no mass transfer equations are solved for the matrix continuum.

Fracture-Rock Matrix Heat Transfer

Two approaches are considered for modeling heat transfer between fractures and rock matrix continua:

Method 1: Spherical Conduction Model.

Analogous to the diffusive mass transport formulation, each computational node in the fracture continuum is coupled to a PDE for heat conduction in spherical rock fragments as

$$\frac{\partial(\rho_m S_m T_m)}{\partial t} = \frac{1}{r^2} \frac{\partial}{\partial r} \left(\lambda_m r^2 \frac{\partial T_m}{\partial r} \right) + E_m \quad (7)$$

where ρ_m is the solid phase mass in the rock matrix per total fracture-matrix volume, S_m is the specific heat of the rock matrix, T_m is the rock matrix temperature, λ_m is the thermal conductivity of the rock matrix, and E_m is the rate of heat generated (+) or absorbed (-) by reactions in the rock matrix at a given radial location and time. Equation (7) is subject to the boundary condition that T_m at the outer radius of the rock fragment is equal to the temperature in the fracture continuum at the corresponding fracture node. Thermal conductivity and heat capacity are computed as a function of kerogen content remaining using empirical formations for Green River oil shale given by Gregg et al. (1981). The heat transfer rate from the matrix to fractures (+) or visa versa (-), H_{fmi} , which is a source-sink term in the fracture heat balance equation, is given by

$$H_{fmi} = E_m - \frac{d\overline{\rho_m S_m T_m}}{dt} \quad (8)$$

where the last term represents the rate of change in stored thermal energy in the matrix.

Method 2: First-Order Heat Transfer Model.

This approach replaces equation (7) with a linear heat transfer function as

$$H_{fm} = \beta(\bar{T}_m - T_f) \quad (9)$$

where β is a heat transfer coefficient, \bar{T}_m is the average rock matrix temperature, and T_f is fracture continuum temperature at the corresponding location. The heat transfer coefficient may be expressed in terms of spherical conduction model parameters in the same manner described for the mass transfer problem, yielding

$$\beta = \frac{15\bar{\lambda}_m}{r_m^2} \quad (10)$$

where $\bar{\lambda}_m$ is the average thermal conductivity in the rock matrix.

Model formulations will be designated by notation of the form Tn-Mm, where n denotes the thermal model method and m represents the mass transfer method, e.g., T1-M1 denotes the most rigorous model using heat transfer formulation 1 and mass transfer method 1.

Analysis of Block Retort Experiments

Description of Experiments

A laboratory study by Gregg et al. (1981), which involved laboratory retorting of a column oil shale having a diameter and height of ~17 cm, will be analyzed first. The block was heated to 900 °C at a constant rate of 18 °C/h in a chamber with a constant flow rate of inert argon gas. Since the block diameter and length were equal and all surfaces were heated and exposed to the gas stream, the block was treated mathematically as a spherical body having an effective spherical diameter computed such that the actual volume-surface area ratio was equal to that of the sphere (i.e., $d_{\text{eff}} = 6 V/A$). The oil shale had a Fischer assay of 23 gal/T (107 L/Mg), and dolomite and calcite weight fractions of 0.38 and 0.082, respectively. The temperature distribution within the rock and the evolution of CO and CO₂ with time were monitored. A second experiment was performed in a similar manner on a block with a diameter of 2.5 cm at

a heating rate of 120 °C/h with measurements of H₂ and CH₄ production.

Simulation Results

Numerical simulations of the large block experiment were performed to assess effects of model formulation on accuracy and computational effort. Computational effort for the various simulation formulations is given in Table 3. Note that the T2-M1 simulation was not performed because temperature-dependent reaction rates and diffusion coefficients cannot be computed at different radial locations for the M1 solution without T1 thermal solution results. A large difference in computational effort occurred between the T1-M1 and T1-M2 solution, primarily because the time-step had to be sharply decreased for the former solution to obtain an accurate solution and even to obtain numerical convergence. In contrast to the sensitivity of computational effort to the mass transfer formulation (specifically M1), predicted oil and gas production rates, mineral decomposition, temperature distributions, etc. were independent of mass transfer model formulation for a given heat transfer formulation. These results indicate that oil shale retorting reactions and fracture-matrix interactions are controlled by heat transfer rather than mass transfer limitations. Note that computational effort as well as numerical results differ very little for T1-M2 vs T1-M3 and for T2-M2 vs. T2-M3 formulations. Therefore, in the remaining of this paper, we focus our attention on effects of thermal model formulation focusing on the T1-M3 and T2-M3 formulations.

Results for T1-M3 and T2-M3 simulations

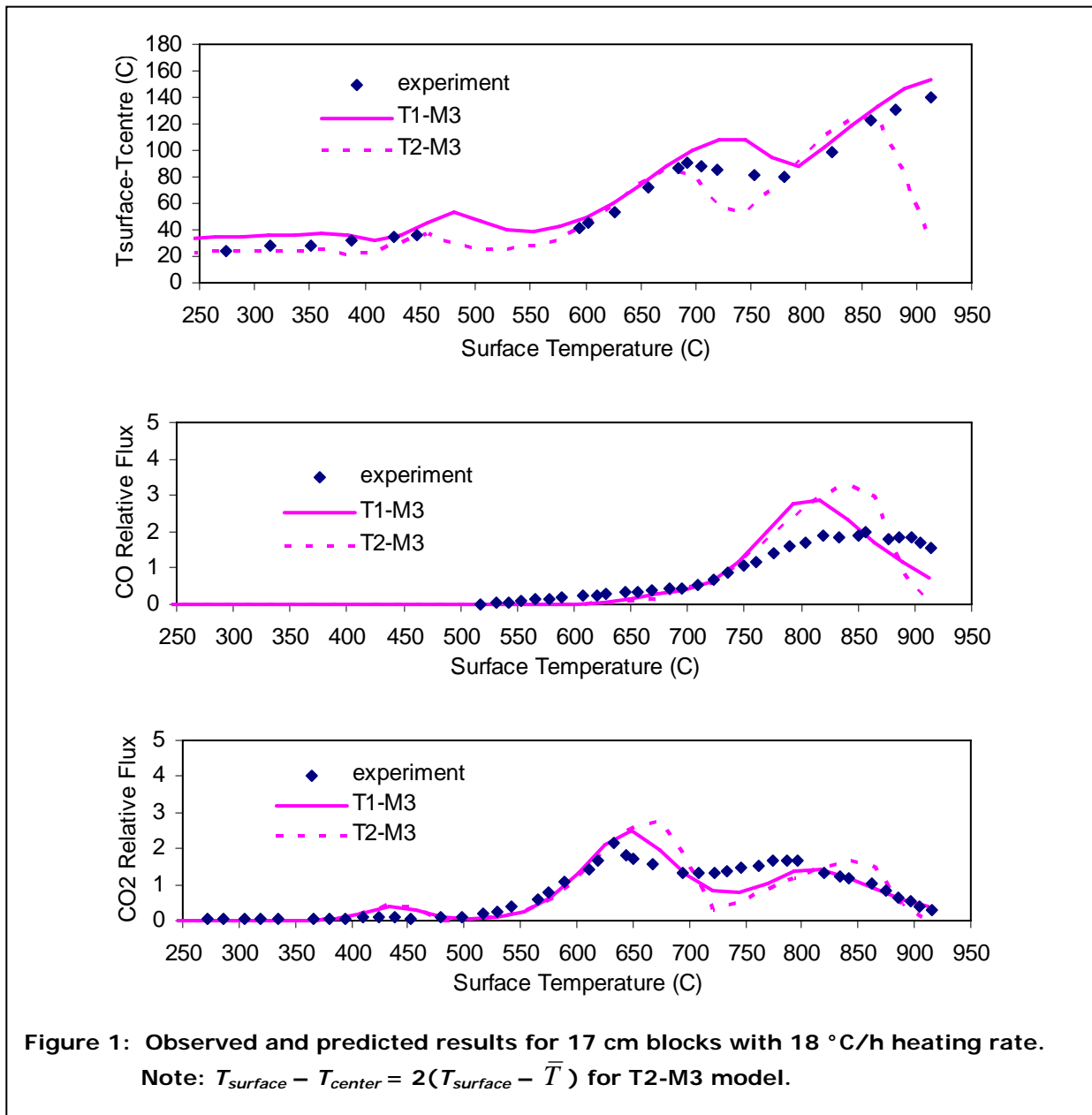
Table 3. CPU time in minutes for simulation of large block experiments using different fracture-matrix mass and heat transfer formulations.

	M1	M2	M3
T1	1200	60	59
T2	n.a.	6.1	6

are compared with experimental data for the large block experiment in Figure 1. Predictions for rock temperature and CO and CO₂ production rates agree somewhat more closely with the observations for the more rigorous T1 model at the expense of approximately an order of magnitude increase in computational effort. Reaction rates tend to peak later and reach completion later. This likely reflects the dispersion in temperatures with the rock predicted by the spherical conduction model.

over time for T1-M3 and T2-M3 simulations are shown in Figure 2 for the small block experiment. The first peak in both plots is due to primary pyrolysis and the broad shoulder at higher temperatures reflects secondary pyrolysis reactions with distributed activation energies. Both the T1 and T2 models agree closely with the observations and exhibit very small differences with each other for the small block experiment.

Predictions of CH₄ and H₂ production rates



Criteria for Applicability of First-Order Approach

While the use of T2 formulations substantially reduces computational effort over T1 formulations, solution accuracy may be sacrificed in some circumstances. We seek now to quantify conditions for which the T2 formulation may be used without loss of accuracy. A number of simulations were performed for block sizes ranging from 2.5 to 20 cm diameter and heating rates from 10 to 100 °C/h using the T1-M3 and T2-M3 formulations. Simulated oil yield as a percent of Fischer assay indicate that T2 solution accuracy diminishes at heating rate and/or block size become large (Figure 3). Deviations between T1 and T2 solutions were quantified by computing the root mean square error (RMSE) of oil yield for each block size and heating rate case from Figure 3. These deviations are plotted in Figure 4 as a function of dimensionless heating rate, R_H , computed as

$$R_H = \frac{d_m^2 r_H \overline{\rho_m S_m}}{\overline{\lambda_m} T_o} \quad (11)$$

where d_m is block diameter, r_H is rate of temperature increase in fractures, T_o is initial rock temperature, and $\overline{\lambda_m} / \overline{\rho_m S_m}$ is the rock thermal diffusivity ($\sim 12 \text{ cm}^2/\text{h}$ for this study). For a distribution of block sizes, the mean squared diameter would be most appropriate to utilize for d_m^2 . A monotonic in-

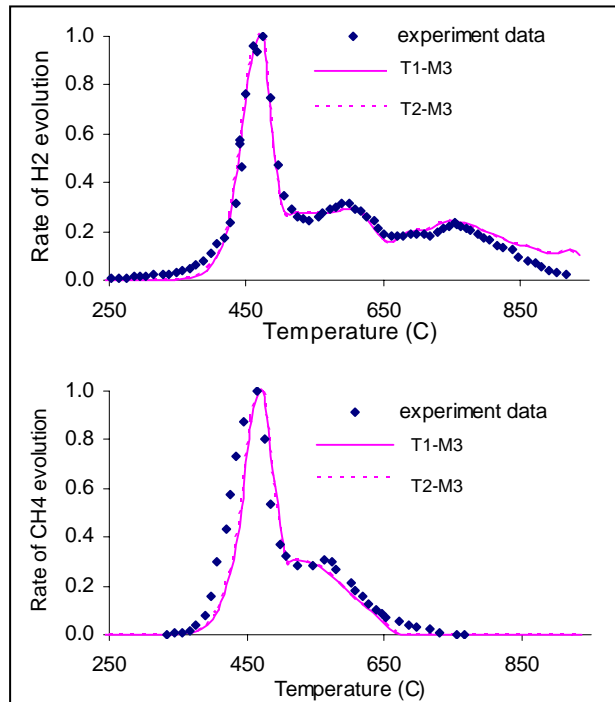


Figure 2: Observed and predicted results for 2.5 cm blocks with 2 °C/h heating rate.

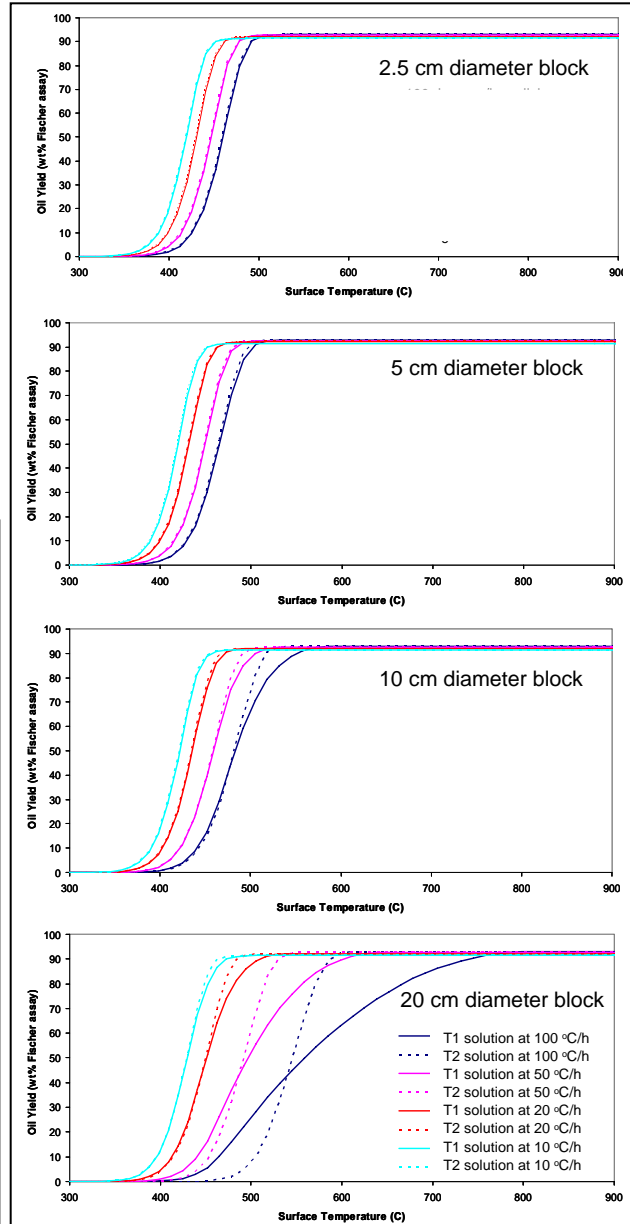
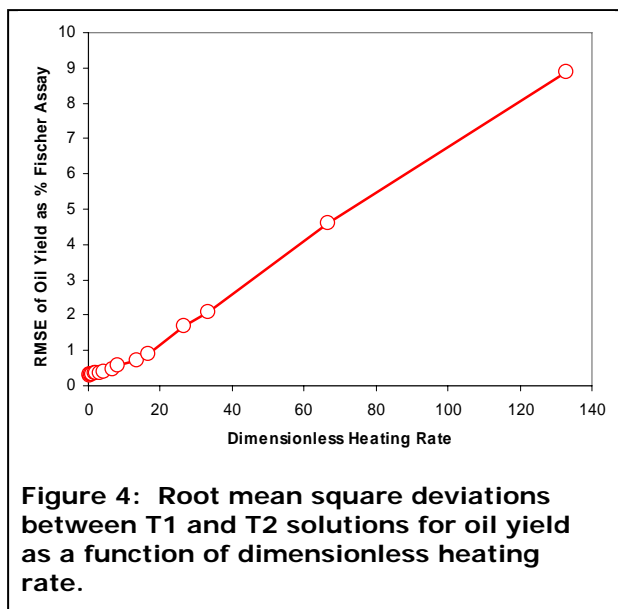


Figure 3: Predicted oil yield for T1 and T2 solutions with various block sizes and heating rates.



crease in T2 prediction error is observed as a function of dimensionless heating rate. For $R_H < 18$, the RMSE of oil yield error is less than 1 percent of Fischer assay, which we propose as a practical criterion for application of the first order heat transfer model.

Summary and Conclusions

Heat and mass transfer rates between permeable fracture porosity and low permeability rock matrix are limited by thermal and mass transport properties of oil shale during in situ retorting. These processes can be modeled using multi-continuum approaches with relevant partial differential equations (PDEs) for transport in fractures and for mass diffusion and heat conduction in the rock matrix. Alternatively, fracture-matrix interactions may be modeled using simple first-order transfer functions that average over the matrix volume, or kinetics of the transfer processes may be disregarded altogether if the rates are sufficiently fast. We present expressions to compute effective first-order heat and mass transfer coefficients explicitly as functions of rock fragment size and known thermal and mass transfer properties, thus avoiding the need for empirical calibration.

The results of this study indicate that thermal disequilibrium is the dominant factor controlling retort reactions, such that

simulation accuracy is unaffected by choice of mass transfer formulation. Computational effort to rigorously simulate diffusive mass transfer in the rock matrix, however, was more than an order or magnitude greater than that required for first-order mass transfer or equilibrium analyses, with no benefit in terms of prediction accuracy. Equilibrium and first-order mass transfer approaches yielded equal accuracy with negligible difference in computational effort. Since the computational price is negligible, it is recommended to use of the first-order approach for its greater rigor, which may be advantageous, for example, if more complex kinetic formulations are employed than used here.

While consideration of non-equilibrium heat transfer between fracture and matrix continua is critical for accurate modeling oil shale retorting, the first-order heat transfer approximation of thermal conduction can be used without significant loss of accuracy if the block size and/or heating rate are not too large, as quantified by a proposed dimensionless heating rate.

Results reported in the paper considered systems with uniform rock fragment size. In practice, fragment size will exhibit significant variability and distributed sizes are unlikely to be well-approximated by simple averaging. Distributed size ranges may be modeled by several discrete block sizes with densities and porosities proportional to their class frequencies. If heat conduction is explicitly modeled for each class, computational effort will increase nearly in proportion to the number of classes. However, negligible additional computational effort would be entailed using the first-order heat transfer approach. Thus, the advantages of the first-order approach will gain even greater significance for realistic simulation of systems characterized by heterogeneous rock fragment distributions.

Acknowledgements

This research was conducted at Oak Ridge National Laboratory (ORNL) with internal support and in conjunction with the Computational Grand-Challenge program at the MSCF in EMSL, a national scientific user fa-

cility sponsored by DOE-OBBER and located at PNNL. ORNL is managed by UT-Battelle LLC for the US Department of Energy under contract DE-AC05-00OR22725.

References Cited

Braun, R. L., 1981, Mathematical Modeling of Modified In Situ and Aboveground Oil Shale Retorting, Lawrence Livermore National Laboratory Report, UCRL-53119, Rev. 1, 46 p.

Braun, R. L., J. C. Diaz, and A. E. Lewis, 1982, Results of mathematical modeling of modified *in situ* oil shale retorting, Proceedings SPE/AIME, SPE 11000.

Campbell, J. H., G. Gallegos, and M. Gregg, 1980, Gas evolution during oil shale pyrolysis. 2. Kinetic and stoichiometric analysis. FUEL, 59, 727-732.

Gregg, M. L., J. H. Campbell and J. R. Taylor, 1981, Laboratory and modeling investigation of a Colorado oil-shale block heated to 900°C, FUEL, 60, 179.

George, J. H. and H. G. Harris, 1977, Mathematical modeling of in situ oil shale retorting, SIAM Numerical Analysis J., 14, 137.

Libicki, S. B. and J. H. Campbell, 1980, Evaluation of retort performance via off-gas and product oil analysis: Geokinetics true *in situ* oil shale retort experiment 17, Lawrence Livermore National Laboratory, Livermore, CA. UCID-18810, 31 p.

Parker, J. C. and A. J. Valocchi, 1986, Constraints on the validity of equilibrium and first-order kinetic transport models in structured soils, Water Resour. Res., 22, 399-407.

Sudduth, B. C., N. W. Merriam, T. F. Turner, P. Vaughn, C. Y. Cha, 1987, Retorting of Non-uniform Oil Shale Rubble, Western Research Institute, DOE/FE/60177-2348.

Tyner, C. E., D. W. Cook, and B. P. Engler, 1985, Oil Shale Pilot Retorting Experiment Summary: Block Permeability Contrast Run 41. Sandia National Laboratories, Albuquerque, NM and Livermore, CA. Sandia Report SAND85-0197, 49 p.

Tyner, C. E. and D. W. Cook, 1984, Oil Shale Pilot Retorting Experiment Summaries: Permeability Contrast Runs 38, 39, and 40. Sandia National Laboratories, Albuquerque, NM and Livermore, CA. Sandia Report SAND83-2650, 44 p.

Yeh, G.T., J.T. Sun, P.M. Jardine, W.D. Burger, Y.L. Fang, M.H. Li, and M.D. Siegel. 2004, HYDROGEOCHEM 5.0: A Three-Dimensional Model of Coupled Fluid Flow, Thermal Transport, and Hydrogeochemical Transport Under Variably Saturated Conditions - Version 5.0, ORNL/TM-2004/107, Oak Ridge National Laboratory, Oak Ridge TN 37831.